Multiple scattering and disorder in extended x-ray-absorption fine-structure analysis

N. Alberding and E. D. Crozier
Department of Physics, Simon Fraser University, Burnaby, British Columbia V5A 1S6, Canada
(Received 22 October 1982)

Analysis of extended x-ray-absorption fine-structure (EXAFS) spectra for non-nearest-neighbor distances must explicitly consider large variations in multiple-scattering effects over the range of thermal motion or static disorder of the positions of the atoms involved. This is illustrated with temperature-dependent data for two μ-oxo-bridged iron compounds with different bridging geometries. Two extreme curve-fitting models assuming different correlations of Fe-Fe distance with bond angle were applied to the data. The model assuming flexible bond angles was better than the model fixing the bond angle. The disparity between the models was greatest for the more linear arrangements of atoms where multiple scattering is sensitive to small displacements. The accuracy of the Fe-Fe distance relative to the x-ray crystallographic result was never better than 0.024 Å. Because the EXAFS amplitude was dominated by the contribution of collinear bridges, the precision was small (+0.02, −0.08 Å) when the bridging angle was within 15° of linearity. The possibility of asymmetry of the Fe-Fe distance distribution was explored in temperature-dependent studies. A negative third central moment of the distribution gave a marginally better fit and a more accurate distance. The origins of this negative moment are discussed.

INTRODUCTION

Extended x-ray-absorption fine-structure (EXAFS) measurements of interatomic distances beyond the first shell of neighbors require a more refined theory than that used for the first shell. For first-shell distances, the analysis needs to include only single scattering of the electron emitted from the x-ray-absorbing atom as it encounters one of its neighboring atoms. Beyond the first shell, there are multiple scattering (MS) pathways between a backscattering atom and an absorbing atom. In this case the single-scattering theory is inadequate.[1–3] The single-scattering formula for the contribution to the EXAFS spectrum of one atom fixed at a distance r from the x-ray absorber is[4]

$$\chi(k)=\frac{|f(k)|}{kr^2}M(k)e^{-2r/\lambda}\sin[2kr+\delta(k)]\ . \tag{1}$$

The momentum wave vector of the photoelectron is k. $|f(k)|$ is the magnitude of the amplitude for backscattering. $\delta(k)$ is the phase shift of the backscattering-absorbing atom pair. The finite lifetime of the photoelectron's final state is included through $\exp(-2r/\lambda)$. Amplitude reduction from multielectron shakeup and shakeoff is included via $M(k)$.[5,6] Teo[7] has shown that multiple scattering from an intervening atom may be included in the single-scattering formula by multiplying the amplitude of $\chi(k)$ by a correction factor $\Omega(\beta,k)$, and adding a correction term, $\omega(\beta,k)$, to the phase

$$\chi(k)=\frac{\Omega(\beta,k)|f(k)|}{kr^2}M(k)e^{-2r/\lambda}\times\sin[2kr+\delta(k)+\omega(\beta,k)]\ . \tag{2}$$

Figure 1 shows the angle β. The corrections depend strongly on this angle, and less critically on the distances r_{AB}, r_{BC}, and r_{AC}.

The total EXAFS spectrum is a superposition of the spectra of individual contributors. Furthermore, thermal disorder or static variations of distances in the bulk sample must be accounted for by integrating over a probability distribution of the positions, $p(\vec{r}_1,\vec{r}_2,\ldots)$:

$$\chi(k)=\int p(\vec{r}_1,\vec{r}_2,\ldots)\sum_i\frac{\Omega(\beta_i,k)|f_i(k)|}{kr_i^2}M(k)\exp(-2r_i/\lambda_i)\sin[2kr_i+\delta_i(k)+\omega(\beta_i,k)]d\vec{r}_1d\vec{r}_2\cdots\ . \tag{3}$$

 ©1983 The American Physical Society

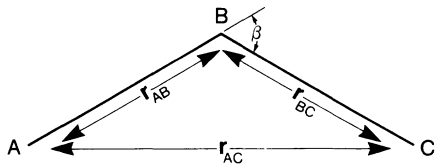

FIG. 1. Arrangement of atoms for which multiple scattering affects the EXAFS determination of the distance r_{AC}. Thermal motion may change the multiple scattering especially if the angle β is near zero.

The index i distinguishes symbols belonging to different atoms. For the single-scattering case, the distances are usually taken to be independent, and often, distributed by a Gaussian. The integral over p then reduces to familiar Debye-Waller terms, $\exp(-2\sigma_i^2 k^2)$. Multiple scattering makes the treatment of disorder more difficult. The angle β_i is an implicit function of the r vectors. As the three atoms involved in the triangular relationship place themselves differently with respect to each other, the multiple-scattering corrections vary. If the atoms are nearly in line, even small displacements may dramatically change the amplitude of $\chi(k)$.[7] The implication is that the MS-correction functions may not be taken out of the integral. In applying his multiple-scattering—correction functions, Teo[7] removed them from the integral and inserted a single-scattering, Gaussian Debye-Waller factor. The MS functions were those of the mean atomic positions. The assumption built into this maneuver, namely β fixed, is not justified in general. Furthermore, the results may be very wrong if the atomic positions make the MS corrections sensitive to small displacements (e.g., nearly collinear bridges).

In this paper we examine the EXAFS of two bimetallic bridged compounds. These compounds and the measurements made on them are described in the experimental section. Two extreme models for the distribution function $p(\vec{r}_1, \vec{r}_2, \ldots)$ and the integration of Eq. (3) are presented: mean multiple scattering and integrated multiple scattering. The analysis section gives the details of these models. The analysis reveals that assumptions on atomic displacements may dramatically affect the structural details deduced from an EXAFS spectrum. In the Appendix it is also indicated that in some bimetallic bridged compounds, the effective two-body metal-metal distribution function may have a negative third central moment which must be explicitly included in EXAFS analysis procedures.

EXPERIMENTAL

The compounds studied are (Fe-HEDTA)$_2$O and (Fe-dipic-OH)$_2$. (HEDTA is ethelyenediamine tetracetic acid; dipic is 2,6-pyridinedicarboxylate.) Their crystallographic structures are known.[8,9] The μ-oxo-bridged iron complex (Fe-HEDTA)$_2$O has each of its iron atoms octahedrally coordinated to oxygen and nitrogen atoms. One oxygen atom is common to the two iron atoms of the dimer and forms the μ-oxo bridge,

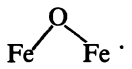

The octahedra are slightly distorted so that the Fe-O-Fe angle is 163.8°. The Fe-Fe distance is 3.554 Å and the Fe-oxo bridging bonds are 1.80 and 1.79 Å.[9]

The dipic structure is also a dimer bridged by two OH groups,

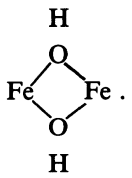

The Fe-Fe distance is 3.089 Å, the bridging angle is 103.4°, and the Fe-OH distances are 1.993 and 1.938 Å.[8]

Powder samples of the two compounds were prepared using published protocols.[9,10] We also grew a single crystal of (Fe-HEDTA)$_2$O about 3×5 mm^2 in cross section. Powder samples were verified by elemental analysis and the crystal's unit-cell dimensions were checked by a rotating crystal pattern. X-ray-absorption spectra were recorded at the Stanford Synchroton Radiation Laboratory on beam line II-2 using the following monochromator crystals: (Fe-HEDTA)$_2$O crystal, Si(111); (Fe-HEDTA)$_2$O powder, Si(111); [dipic(H_2O)FeOH]$_2$, Si(220). The spectra were measured at 80 and 295 K.

ANALYSIS

Spectra of oriented single crystals of (Fe-HEDTA)$_2$O helped identify the iron peak. Two orientations of the crystal with respect to the electric field polarization of the incident x-ray beam were chosen. The iron shell was most predominant in the spectra when the polarization lay parallel to the iron-iron axis, whereas its contribution was absent when the polarization was perpendicular to this direction. By comparing the Fourier transforms of the two orientations the iron shell was readily identified (Fig. 2).

For quantitative analysis, data from the (Fe-HEDTA)$_2$O powder samples were more useful than the crystalline data because of the better signal-to-noise ratio at high-k values. The better signal-to-noise ratio of the powder sample might be attributed

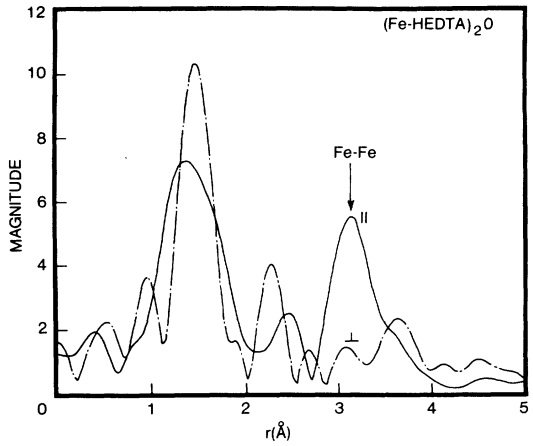

FIG. 2. Magnitudes of the Fourier transforms of the EXAFS spectrum of an oriented single crystal of (Fe-HEDTA)$_2$O at 293 K. Solid line: Electric polarization of the beam parallel to the Fe-Fe direction. Dot-dashed line: Polarization perpendicular to the Fe-Fe direction. The transforms are of $k^3\chi(k)W(k)$; windows are 3.31–12.41 Å^{-1}. $W(k)$ is a 10% Gaussian window.

to a larger cross section of the sample exposed to the beam or to a better thickness of the powder sample.

The EXAFS spectrum $\chi(k)$ was obtained from the absorption spectrum using traditional methods.[11] The Fourier transform of $\chi(k)$ is a function of r resembling the radial distribution of atoms surrounding the x-ray absorber. In the case of (Fe-HEDTA)$_2$O, the range in r containing the iron's contribution was determined by comparing the transforms of the oriented crystal spectra with the spectrum in question. Setting all components of the transform outside this range to zero and then taking the inverse transform produced a k-space spectrum containing only the contribution of the isolated peak. At this point, curve fitting was used to determine the parameters of interest. Table I indicates the transform windows used. The function transformed was $k^3\chi(k)W(k)$, where $W(k)$ was a 10% Gaussian window which could be removed in later analysis. With a k-space transform window of 2.8–17 Å^{-1} a nearby carbon shell could not be separated from the iron shell. However, because carbon's backscattering predominates at low k while iron's is large at high k, the two shells could be separated in k space. Using two-shell simulations, we verified that the carbon's contribution above 7 Å^{-1} was small. Only the iron-iron parameters needed to be considered in the spectrum above 7 Å^{-1}.

Having EXAFS data on these two compounds we can explore how different models of the correlated motions of atoms involved in multiple scattering affect the structure deduced from analysis of the spectrum. We have compared two extreme assumptions about the correlation of the bridging systems.

(1) The first model assumes that the Fe-Fe distance varies only because of the stretching of Fe–O bonds, leaving the angle β unchanged. The multiple-scattering corrections remain virtually constant over the distribution of atomic positions. Thus Ω and ω may be removed from the integration of Eq. (3), and the disorder can be accounted for in the same manner as in single scattering. Teo implicitly used this treatment.[7] It would be valid in two situations: (i) Ω and ω do not vary with β and interatomic distances or (ii) β is fixed. Since here the multiple-scattering corrections take on the values they have at the atoms' mean positions, we call this the mean multiple-scattering (MMS) approach.

(2) The second model assumes that all the variation of $r_{\text{Fe-Fe}}$ comes from bending the bond angle, while the bond lengths are constant. Though still an idealization, this model is probably more reasonable than the previous one: Relatively less energy is needed to bend the Fe-O-Fe system than to stretch the Fe–O bonds. Such a "rigid-hinge" model necessitates leaving the MS corrections inside the integral of Eq. (3) since they change over the distribution of atomic positions. This approach will be dubbed integrated multiple scattering (IMS).

To integrate Eq. (3) numerically, a discrete probability distribution of r_{AC} was used to model the disorder of the distance. The angle β was then calculated assuming that r_{AB} and r_{BC} were fixed:

$$\beta = 180° - \cos^{-1}\left[\frac{r_{AB}^2 + r_{BC}^2 - r_{AC}^2}{2r_{AB}r_{BC}}\right]. \quad (4)$$

The discrete probability distribution that we used was derived from the Gaussian distribution evaluated at nine points,

TABLE I. Transform windows used in analyzing the data.

	(Fe-HEDTA)$_2$O	(Fe-dipic-OH)$_2$O
k-space range of transform	2.81–17.01 Å^{-1}	2.34–19.97 Å^{-1}
R-space filter window	2.34– 4.43 Å	2.16– 3.24 Å
k-space range used in fit	7.20–15.11 Å^{-1}	8.06–15.07 Å^{-1}

$$r_j=(\sigma^2/2)^{1/2}(j-5)+\bar{r},\quad j=1,\ldots,9$$
$$p(r)\Delta r\equiv P_j=(1/\sqrt{4\pi})\exp[-(j-5)^2/4]\ , \tag{5}$$

where $\bar{r}$ is the mean distance and σ^2 is the mean-square deviation in r. The spectrum simulated for one shell is then

$$\chi(k)=\sum_{j=1}^{9} P_j\frac{\Omega(\beta_j,k)\,|f(k)|}{kr_j^2}M(k)\exp(-2r_j/\lambda)$$
$$\times\sin[2kr_j+\delta(k)+\omega(\beta_j,k)]\ . \tag{6}$$

In tests assuming single scattering and a Gaussian distribution, summing the discrete nine-point distribution produced a spectrum practically indistinguishable from the analytical form. The difference in $k\chi(k)$ was less than 10^{-4} Å^{-1}.

To simulate the IMS model, the multiple-scattering corrections were calculated at each r_j, whereas in the MMS they were fixed at the mean value of r. A nonlinear least-squares fitting program[12] varied the parameters of the model to fit the data. The parameters varied were ΔE_0, the deviation of the inner potential from the inflection point of the absorption edge, η, the mean-free-path parameter where the mean free path is $\lambda=k^2/\eta$, and σ^2, the standard deviation of the distribution in r_{AC}. In order to correspond to Teo's work, we parametrized λ as above rather than use other possible functional forms.[13] To reduce the number of variables, the number of backscattering atoms was fixed at unity as was the multielectron function $M(k)$, even though $M(k)$ is known to have a k dependence.[13,14]

In exploring the applicability of the two models we fixed $r_{\text{Fe-Fe}}$ at various values and sought the best fit by varying ΔE_0, η, and σ^2. The goodness of fit (GOF) was measured by the formula

$$\sum_{n=1}^{\text{No. pts.}}[\chi^{\text{simulated}}(k_n)-\chi^{\text{expt}}(k_n)]^2/E\ . \tag{7}$$

When E approximates the mean-square amplitude of the noise in $\chi(k)$, a "good fit" should make GOF near or less than unity. In our fits we estimated E to be 0.001. GOF is plotted as a function of $r_{\text{Fe-Fe}}$ in Fig. 3 for the (Fe-HEDTA)$_2$O data taken at room temperature. The solid line represents the IMS model and the dashed lines the MMS model. In both cases the iron—to—bridging-oxygen bond lengths $r_{\text{Fe-O}}$ and $r_{\text{O-Fe}}$ were set at the crystallographically determined distances 1.80 and 1.79 Å.[10] While $r_{\text{Fe-Fe}}$ was the independent variable, we allowed its value to exceed the sum $r_{\text{Fe-O}}+r_{\text{O-Fe}}$. When this happened the linear bridge could "stretch" so the $r_{\text{Fe-O}}$ and $r_{\text{O-Fe}}$ distances were both set equal to $r_{\text{Fe-Fe}}/2$. Table II lists the parameters that produced the best fits.

We also tried using the angle β as an independent variable instead of $r_{\text{Fe-Fe}}$, letting the angle have a Gaussian distribution. No acceptable fit resulted.

When the MMS model was applied to the EXAFS of (Fe-HEDTA)$_2$O, the best fit occurred at $r_{\text{Fe-Fe}}=3.63$ Å. This implies a linear arrangement and disagrees completely with the crystallographic result 3.55 Å. The main problem was the inability of the MMS model to match the amplitude of the experimental $\chi(k)$. No acceptable fit could be found at a distance near 3.55 Å. The IMS approach, on the other hand, produced a good fit in the right range of the interiron distances. However, the precision with which one could determine the distance from the EXAFS fit alone is limited to within 0.1 Å because the minimum in GOF is broad and shallow.

One can see the reason for the difference in the amplitudes predicted by the IMS and MMS simulations. Figure 4 compares a typical distribution in $r_{\text{Fe-Fe}}$ with $\Omega(\beta,k)$ over the same range for (Fe-HEDTA)$_2$O at $k=10$ Å^{-1}. Because Ω varies dramatically over the range of the distribution, the product $P(r_{\text{Fe-Fe}})\Omega(\beta,k)$ is very different than if β were fixed at its mean value.

It should be noted that the effect of the asym-

TABLE II. Best-fit parameters for room-temperature data using both mean multiple-scattering and integrated—multiple-scattering models. A Gaussian distribution in r_{AC} is assumed.

	r_{AC} (Å)	β	ΔE_0 (eV)	σ^2 (Å^2)	η (Å^{-3})	GOF
(Fe-HEDTA)$_2$O						
MMS	3.630	0.0°	10.28	0.0050	21.5	0.57
IMS	3.579	9.0°	12.00	0.0142	16.7	1.24
(Fe-dipic-OH)$_2$						
MMS	3.130	74.5°	9.49	0.0020	23.5	1.33
IMS	3.128	74.6°	8.72	0.0019	23.8	1.34

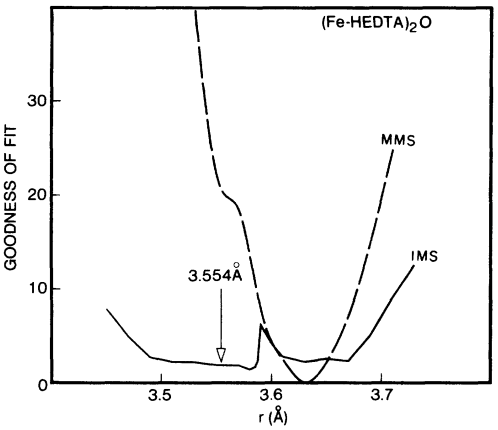

FIG. 3. Goodness-of-fit parameter for the fits to $(Fe\text{-}HEDTA)_2O$ at room temperature as a function of $r_{Fe\text{-}Fe}$. The dashed line was obtained assuming that the multiple-scattering corrections were those of the atomic positions averaged over the entire thermal and static distribution of the oxygen-atom positions (mean multiple scattering). The solid line is for fits which take into account changes in the multiple-scattering correction over the distribution of positions (integrated multiple scattering). The arrow indicates the Fe-Fe distance 3.554 Å, obtained by x-ray diffraction (Ref. 10).

metry in the product $P(r)\Omega(\beta,k)$ is, in a sense, similar to the more commonly discussed case of asymmetry in the distribution function of nearest neighbors,[11,14,16] causing a modification of the amplitude and the introduction of an additional term $\Sigma(k)$ in the phase of $\chi(k)$. In the MMS model $\Sigma(k)$ is omitted and an error in the bond length can occur. By inserting a $\Sigma(k)$ varying as k^3 we were able to force the MMS model to converge to the known crystallographic Fe-Fe distance.[15] However, the complexity of the product $P(r)\Omega(\beta,k)$ as a function of r would seem to preclude generally using such a simple functional form for $\Sigma(k)$.

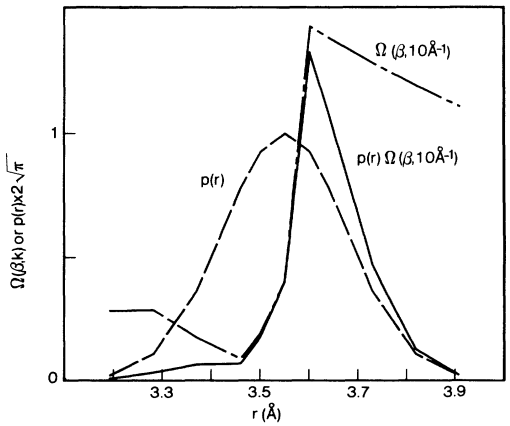

FIG. 4. Illustration of the effect of multiple scattering on the amplitude of EXAFS of nearly linear bridges. Dashed line: a Gaussian $p(r)$. Dot-dashed line: $\Omega(\beta,k=10\ \text{Å}^{-1})$ for $r_{AB}=1.79$ Å, $r_{BC}=1.80$ Å, $\beta=16°$. Solid line: the product $P(r)\Omega(\beta,k)$. This product mimics an asymmetric $p(r)$ and thus also distorts the phase of $\chi(k)$ (Ref. 15).

The IMS fits the amplitude better because it allows multiple scattering to amplify the backscattering when the atoms line up. In effect, the EXAFS mainly "sees" any minority of bridges which are linear and disregards nonlinear bridges even though they are more numerous. This may explain the insensitivity of the fits to interatomic distance in this case.

On the other hand, in the $(Fe\text{-}dipic\text{-}OH)_2$ complex the value of β is 76.4° as opposed to 16.2° in $(Fe\text{-}HEDTA)_2O$, so that collinearity of the atoms is not likely. Consequently, both the IMS and MMS models converge to about the same result. In obtaining the results shown in Figs. 5(a)–5(c), the two iron-hydroxyl distances were fixed at 1.993 and 1.938 Å, respectively, these being the crystallographically determined distances.[9] Figure 5(a) shows GOF vs $r_{Fe\text{-}Fe}$ in this case and Fig. 5(b) shows a typical fit. For both models the best-fit Fe-Fe distance is larger than the reported distance. The discrepancy may be due to various causes:

(1) different forward scattering amplitudes for the bridging hydroxyl groups of $(Fe\text{-}dipic\text{-}OH)_2$ versus the oxygen atom of $(Fe\text{-}HEDTA)_2O$;

(2) additional multiple-scattering pathways from the double bridge;

(3) asymmetry of the $r_{Fe\text{-}Fe}$ distribution (see Appendix).

To test for an asymmetric distribution we first analyzed data taken at 80 K where the effects of an asymmetric thermal distribution should be reduced compared to 295 K. The low-temperature spectrum was fit assuming a Gaussian distribution. ΔE_0 and η were then fixed at the values obtained and the 295-K data were fit with an asymmetric distribution. The results are listed in Table III. For the room-temperature data we used an *ad hoc* form for the distribution,

$$p(r)=\frac{1}{Z}\exp(-y^2/2\sigma^2)\ , \qquad y=(r-r_p)\exp[a(r-r_p)]\ , \tag{8}$$

where r_p is the peak of the distribution and

$$Z=\int_{-\infty}^{\infty}\exp(-y^2/2\sigma^2)dr\ .$$

This distribution is Gaussian for $a=0$, $a>0$ skews the distribution above its peak, and $a<0$ skews it below the peak. The third central moment of the

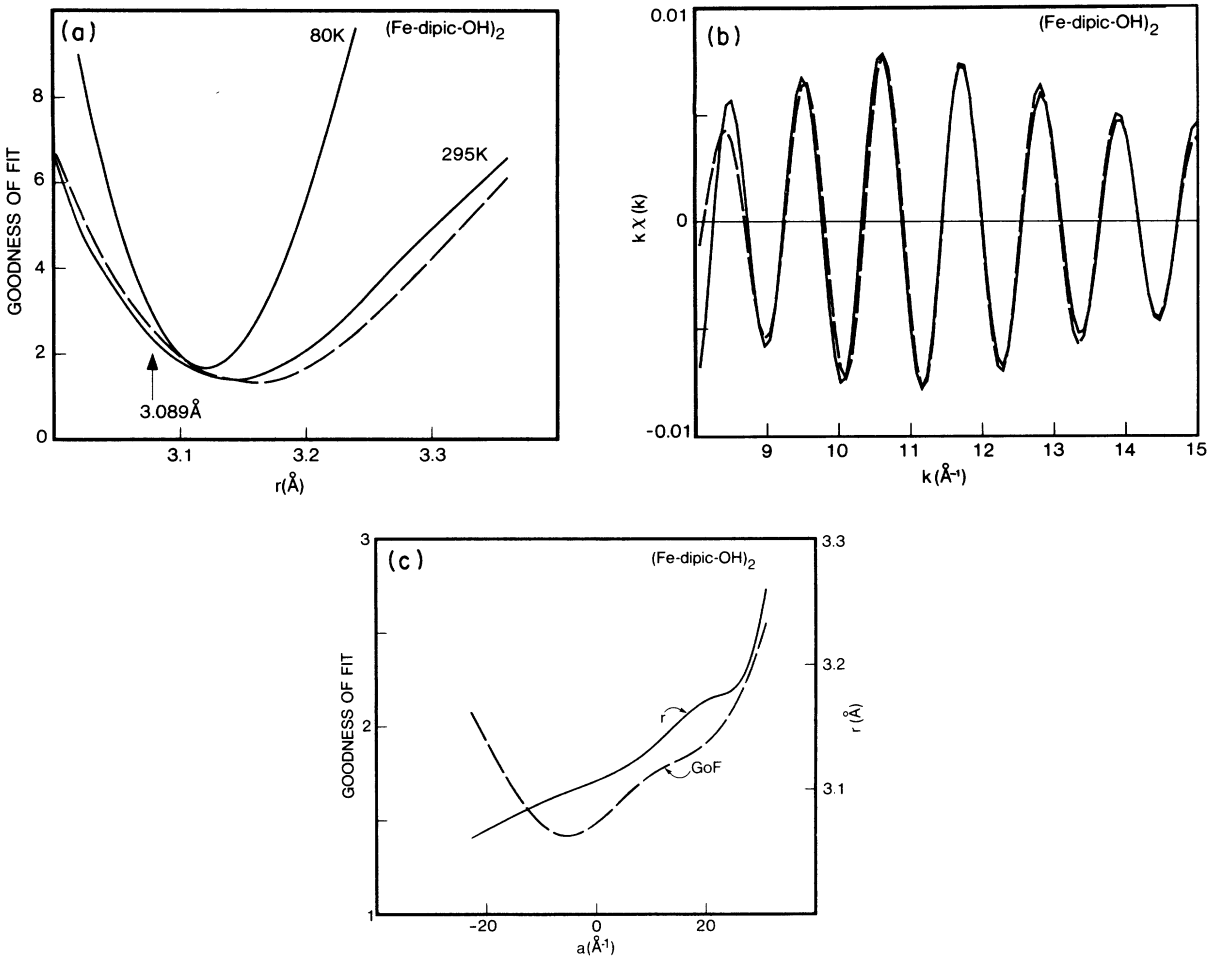

FIG. 5. (a) Goodness-of-fit parameter for the $(Fe\text{-}dipic\text{-}OH)_2$ data. The solid lines are for the integrated multiple-scattering model on 80- and 295-K data. The dashed line represents the mean multiple-scattering model at 295 K. A Gaussian distribution was assumed for $r_{Fe\text{-}Fe}$. The arrow indicates the Fe-Fe distance 3.089 Å, obtained by x-ray diffraction (Ref. 9). (b) Best fit (dashed line) to the $(Fe\text{-}dipic\text{-}OH)_2$ iron shell (solid line) taken at 295 K. The parameters are those of Table II (IMS). (c) Asymmetry in $(Fe\text{-}dipic\text{-}OH)_2$. The dashed line is the goodness of fit to $(Fe\text{-}dipic\text{-}OH)_2$ room-temperature data as a function of the asymmetry of the distribution of $r_{Fe\text{-}Fe}$ given by parameter a. ΔE_0 and η (the mean-free-path parameter) were fixed from the fits to the liquid-nitrogen—temperature data. The solid line shows the correlation of the mean $r_{Fe\text{-}Fe}$ with the asymmetry parameter.

TABLE III. Fits to $(Fe\text{-}dipic\text{-}OH)_2O$ where an asymmetric distribution of $r_{Fe\text{-}Fe}$ was introduced. Here ΔE_0 and η were determined by the best fit to the liquid-nitrogen—temperature data using a Gaussian distribution. The room-temperature data was fit using these values of ΔE_0 and η and the distribution was allowed to become asymmetric through a nonzero value of a. The integrated multiple-scattering model was used. Values in parentheses were fixed.

Temp.	r_{AC} (Å)	β	ΔE_0 (eV)	σ^2 (Å^{-2})	η (Å^{-3})	a (Å^{-1})	GOF
80 K	3.110	75.4°	2.46	0.000 426	22	(0)	1.67
295 K	3.096	76.1°	(2.46)	0.001 88	(22)	−6.45	1.42

distribution has the same sign as a. The discrete version used in the fitting routine used the same P_j values given by Eq. (5), but at positions

$$r_j=[(\sigma^2/2)^{1/2}(j-5)]\exp[a(\sigma^2/2)^{1/2}(j-5)] +r_p,\quad j=1,\ldots,9\ .$$

The GOF to the (Fe-dipic-OH)$_2$ data as a function of the asymmetry parameter a is plotted in Fig. 5(c). The value of a giving the best fit is -6.44 ± 16 Å, making

$$\langle(r-\bar{r})^3\rangle=-0.000\,214$$

in units of Å^3. The strong correlation of $\bar{r}$ with a is also illustrated in Fig. 5(c). Eisenberger and Brown,[16] Rehr,[17] Bunker,[18] and Crozier and Seary[11] examined theoretically and experimentally the effect of asymmetry in the simple-scattering case. The correlation we find is analogous. Though allowing asymmetry in the room-temperature fits of (Fe-dipic-OH)$_2$ gives a value of $r_{\text{Fe-Fe}}$ closer to the crystallographically determined value, the insensitivity to a rules out asserting that it is nonzero.

CONCLUSIONS

Teo[7] has shown that the sensitivity of the amplitude and phase of the EXAFS interference function $\chi(k)$ to multiple scattering provides a potential quantitative method of determining bond angles in chemical compounds. We found that in at least one class of compounds, μ-oxo-bridged iron complexes, allowance must be made for large variations in multiple-scattering effects arising from dynamic fluctuations in bond angles due to thermal motion. Static disorder in the positions of the atoms involved would have a similar effect. These considerations are very important when the intervening atom responsible for the multiple scattering is nearly in line with the backscattering and absorbing atoms.

A curve-fitting method was developed and applied to two extreme models: a mean multiple-scattering model in which the bond angle was rigid and an integrated multiple-scattering model in which the bond angle was permitted to flex. The latter model produced more accurate results for (Fe-HEDTA)$_2$O giving a bond angle $171.0^{+9^\circ}_{-17^\circ}$ deg. and Fe-Fe separation of $3.579^{+0.02}_{-0.08}$ Å relative to the crystallographically determined values 163.8° and 3.554 Å. The compound (Fe-dipic-OH)$_2$ has an equilibrium bond angle of 103.4°; therefore, collinear arrangements of atoms were less important and both models converged to about the same result, $105.4^\circ\pm2.0^\circ$.

In the case of (Fe-dipic-OH)$_2$ we allowed the fitting program to introduce an asymmetric distribution of non-nearest-neighbor distances. This led to a distribution with a negative third central moment, the origins of which are discussed in the Appendix. Though a marginally better fit resulted with a distance closer to the crystallographic distance, this analysis was too insensitive to the amount of asymmetry to be definitive.

The data analysis of other molecular complexes may require different models for the correlation of the positions of atoms involved in multiple scattering. Finding the correct model is an important step in the analysis.

When multiple scattering is important, the phase of a simulated $\chi(k)$ cannot be calculated independently of its amplitude because of the strong asymmetry in r of the product $P(r)\Omega(\beta,k)$. This asymmetry modifies the phase in a manner similar to an asymmetric distribution of nearest-neighbor distances. If one wishes to eliminate uncertainties arising from the amplitude model by fitting only the phase, Fourier extraction of the phase from each simulated $\chi(k)$ would be necessary. This would considerably lengthen the fitting process.

Some investigators recommend using empirical phase and amplitude functions derived from well-characterized model systems rather than taking theoretical functions. Where multiple scattering exists, the total amplitude factor and phase shifts depend on the relative positions of the atoms as well as their chemical nature. Therefore, unless the geometry of the model system exactly matches that of the unknown system, a direct transfer of phase and amplitude functions is not correct. A possible solution to the problem would be to use the theoretical multiple-scattering functions of Teo to correct empirical functions for changes in geometry of the unknown system as well as differences in dynamic and static disorder.

Note added in proof. It has been brought to our attention that a more accurate multiple-scattering expression has recently been published by J. J. Boland, S. E. Crane, and J. D. Baldeschwieler in J. Chem. Phys. 77, 142 (1982). Their expression includes a geometrical factor $3(\hat{e}\cdot\hat{r}_{AB})(\hat{e}\cdot\hat{r}_{AC})$ in the amplitude of the term corresponding to the scattering path $A\rightarrow B\rightarrow C\rightarrow A$, which for polycrystalline samples average to $\hat{r}_{AB}\cdot\hat{r}_{AC}$. The second term of Eq. (10) in Ref. 7 omits this factor. Upon including the correction, we found that the amplitude of the calculated spectrum changed by about 3% in the case of (Fe-dipic-OH)$_2$ and by only 1% in the case of (Fe-HEDTA)$_2$O. Such a minor effect is expected since, for these compounds, the second term is small when the geometrical factor is significantly less than

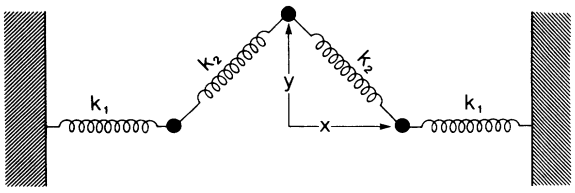

FIG. 6. Simple spring model for the potential energy of a bridged system.

unity. The results and conclusions of the present paper are unaffected.

ACKNOWLEDGMENTS

The authors would like to thank S. Grewal for preparing the samples, A. J. Seary for his assistance in data analysis, D. Sutton for useful discussions, and the staff of the Stanford Synchrotron Radiation Laboratory for making the experimental work possible. N. Alberding received a Simon Fraser University research associateship during this project. The research was partially funded by a grant from the Natural Science and Engineering Research Council of Canada. Work done at the Stanford Synchrotron Radiation Laboratory is supported by the National Science Foundation through the Division of Materials Research and the National Institutes of Health through the Biotechnology Research Program in the Division of Research Resources in cooperation with the U.S. Department of Energy.

APPENDIX

A pair distribution function whose third central moment is negative may need some discussion. Common interatomic potentials such as the Lennard-Jones or Morse potentials would produce a positive third moment because of their repulsive "hard cores" and "soft" attractive tails. In bridged systems we can justify this being reversed, the effective two-body potential being harder at larger r than smaller r. Several considerations may be relevant:

(1) A harmonic potential for the bond angle, thus a Gaussian distribution in β, can be related to the distribution in r_{AC} through Eq. (3). This distribution in r_{AC} has $\langle (r-\bar{r})^3 \rangle < 0$ for $\beta < 90°$.

(2) The double OH bridge of $(\text{Fe-dipic-OH})_2$ is "sterically hindered" from becoming linear as the two hydroxyl groups bump into each other.

(3) The spring model of Fig. 6 gives an asymmetric pair distribution. The coordinates of interest are x, the distance of the iron from the midpoint, and y, the deviation of the oxygen atom from the iron-iron axis.

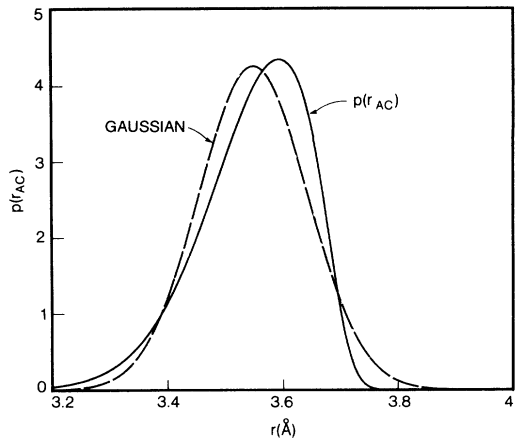

FIG. 7. A-C pair distribution function derived from the model of Fig. 6 (solid line) compared to a Gaussian distribution with the same standard deviation and mean (dashed line).

The potential energy in these coordinates is

$$V(x,y)=k_1(x-a)^2+k_2[(x^2+y^2)^{1/2}-b]^2 , \tag{A1}$$

where a is the equilibrium position of the iron atoms and b is the equilibrium Fe—O bond length. We are interested in the thermal distribution of coordinate x given by Maxwell-Boltzmann statistics,

$$p(x)=(1/Z)\int \exp[-\beta V(x,y)]dy , \tag{A2}$$

where

$$Z=\int_{-\infty}^{\infty}\int_{-\infty}^{\infty}\exp[-\beta V(x,y)]dx\,dy .$$

The pair distribution is the convolution

$$p(r)=\int p(r-x)p(x)dx . \tag{A3}$$

Only the symmetric configuration is considered because, for a given r, it has the least energy and is the most probable.

From this model we have calculated $P(r)$ numerically, choosing values for k_1 and k_2 based on published infrared stretching frequencies.[19] At temperatures near 295 K, $k_1\beta=40$ and $k_2\beta=100$. (Here β is the inverse temperature in energy units.) The distribution that results is compared to a Gaussian distribution in Fig. 7. Its third central moment is $-0.000\,54$ Å^3.

[1]P. A. Lee and J. B. Pendry, Phys. Rev. B 11, 2795 (1975).
[2]C. A. Ashley and S. Doniach, Phys. Rev. B 11, 1279 (1975).
[3]P. A. Lee and G. Beni, Phys. Rev. B 15, 2862 (1977).
[4]E. A. Stern, Phys. Rev. B 10, 3027 (1974).
[5]J. J. Rehr, E. A. Stern, R. L.Martin, and E. R. Davidson, Phys. Rev. B 17, 560 (1979).
[6]E. A. Stern, S. M. Heald, and B. Bunker, Phys. Rev. Lett. 42, 1372 (1979).
[7]B. K. Teo, J. Am. Chem. Soc. 103, 3990 (1981).
[8]S. J. Lippard, H. Schugar, and C. Walling, Inorg. Chem. 6, 1825 (1967).
[9]J. A. Thich, C. C. Ou, D. Powers, B. Vasilou, D. Mastropaolo, Joseph A. Potenza, and H. Schugar, J. Am. Chem. Soc. 98, 1425 (1978).
[10]H. Schugar, C. Walling, R. B. Jones, and H. B. Gray, J. Am. Chem. Soc. 89, 3712 (1967).
[11]E. D. Crozier and A. J. Seary, Can. J. Phys. 58, 1388 (1980).
[12]F. James and M. Roos, Computer Code MINUIT (CERN, Geneva, 1977), version 2.77.
[13]E. A. Stern, B. Bunker, and S. M. Heald, Phys. Rev. B 21, 5521 (1980).
[14]E. D. Crozier and A. J. Seary, Can. J. Phys. 59, 876 (1981).
[15]N. Alberding, E. D. Crozier, and A. J. Seary, Stanford Synchrotron Radiation Laboratory Report No. 81/02 (unpublished).
[16]P. Eisenberger and G. S. Brown, Solid State Commun. 29, 481 (1979).
[17]J. J. Rehr (unpublished).
[18]Grant Bunker, Nucl. Instrum. Methods (in press).
[19]K. Nakamura, *Infrared and Raman Spectra of Inorganic and Coordination Compounds,* 3rd ed. (Wiley, New York, 1978).